LBL-33661

The Role of Fault Zones in Affecting Multiphase Flow at Yucca Mountain

Y. W. Tsang, K. Pruess, and J. S. Y. Wang

Earth Sciences Division
Lawrence Berkeley Laboratory
University of California
Berkeley, California 94720

January 1993

This work was supported by the Director, Office of Civilian Radioactive Waste Management, Yucca Mountain Site Characterization Project Office, Regulatory and Site Evaluation Division, under U.S. Department of Energy Contract No. DE-AC03-76SF00098.

ABSTRACT

Within Yucca Mountain, the potential High Level Nuclear-Waste Repository site, there are large scale fault zones, most notably the Ghost Dance Fault. The effect of such high-permeability, large-scale discontinuities on the flow and transport is a question of concern in assessing the ability of the site to isolate radio-nuclides from the biosphere. In this paper, we present a numerical study to investigate the role of the fault in affecting both the liquid and gas phase flows in the natural state at Yucca Mountain prior to waste emplacement, as well as after the waste emplacement when the fluid flow is strongly heat-driven. Our study shows that if the characteristic curves of the Ghost Dance Fault obey the same relationship between saturated permeability and capillary scaling parameter, as is observed from the measured data of Yucca Mountain welded and nonwelded tuffs, Apache Leap tuffs, and Las Cruces soil, then a large saturated permeability of the Ghost Dance Fault will play little role in channeling water into the fault, or in enhancing the flow of water down the fault. However, the Fault may greatly enhance the upward gas flow after emplacement of waste. This may have implications on the transport of gaseous radio-nuclides such as C^{14}.The results of this study also focus attention on the need for field measurements of fluid flow in the fault zones.

INTRODUCTION

The potential High Level Nuclear-Waste Repository is sited in the partially saturated densely fractured welded tuffs at Yucca Mountain. In the event of a breach in the engineered barrier, the ability of the natural system to contain the waste would rely on the fact that, at capillary equilibrium, the liquid mostly resides in the tuff matrix which has extremely low permeability. The fractures, though having absolute permeability many orders higher than the matrix, are practically drained of water and therefore play little role in the transport of any released radio-nuclides in the liquid phase. In addition to small scale fractures in the welded tuff units, there are also large scale fault zones within the Yucca Mountain area. Most notably there is the Ghost Dance Fault, which is located within the potential repository site, and which can be traced at the surface and is believed to extend down from the surface past the repository depth, perhaps all the way to the water table. Since high absolute permeability may be attributed to such zones of large scale discontinuity, the effect of the fault on the flow and transport is a question of great concern in assessing the ability of the site to isolate radio-nuclides from the biosphere. At present the USGS is conducting a field study of detailed geologic mapping and surface fracture mapping to better characterize the Ghost Dance Fault.[1] In this paper, we present a numerical study to investigate the role of the fault in affecting both the liquid and gas phase flows in the natural state at Yucca Mountain prior to waste emplacement, as well as after waste emplacement when the fluid flow will be strongly heat-driven.

MODELING APPROACH

To study the effect of a fault on flow at Yucca Mountain, we model a two dimensional east-west vertical section (Figure 1). This model provides a schematic representation of hydrological features such as the inter-layering of the nonwelded porous tuff units Paintbrush (PTN) and Calico Hills (CHN), and the welded fractured-porous units Tiva Canyon (TCW), Topopah Spring (TSW) and Prow Pass (PPW). It also accounts for the tilting of the layers, and the irregular surface topography. In designing the calculational grid for this model, fine gridding in columns 11 through 15 over a width of 80 m is used to represent the Ghost Dance Fault. Through suitable choice of hydrologic parameters such as permeability, porosity, relative permeability and capillary suction characteristic curves for these columns, the Ghost Dance Fault is schematically represented. The potential repository extends over a length of 1590 m from columns 1 through 16 in the tilted center section and is represented by the thinnest layer of thickness 4.5 m, the height of a waste package within the Topopah Spring Unit. Hydrological parameters for the different welded and nonwelded tuff units are available from laboratory measurements,[2,3] but we are unaware of any parameter measurements for the faults. The lack of hydrological data for faults is one of the reasons that little is known of their role in affecting flow at Yucca Mountain. To arrive at some estimates of the hydrological parameters for the fault, we take our starting point from the work of Wang,[4] who made a study of the available data of the saturated and unsaturated flow parameters of Yucca Mountain and Apache Leap tuffs as well as the Las Cruces soil. The characteristic curves have been represented with the van Genuchten model:

$$S_e = \left[1 + (|\alpha h|)^n\right]^{-m} \qquad (1)$$

where α, n, m are empirical parameters and S_e is the effective liquid saturation

$$S_e = \frac{(S - S_r)}{(S_s - S_r)} \qquad (2)$$

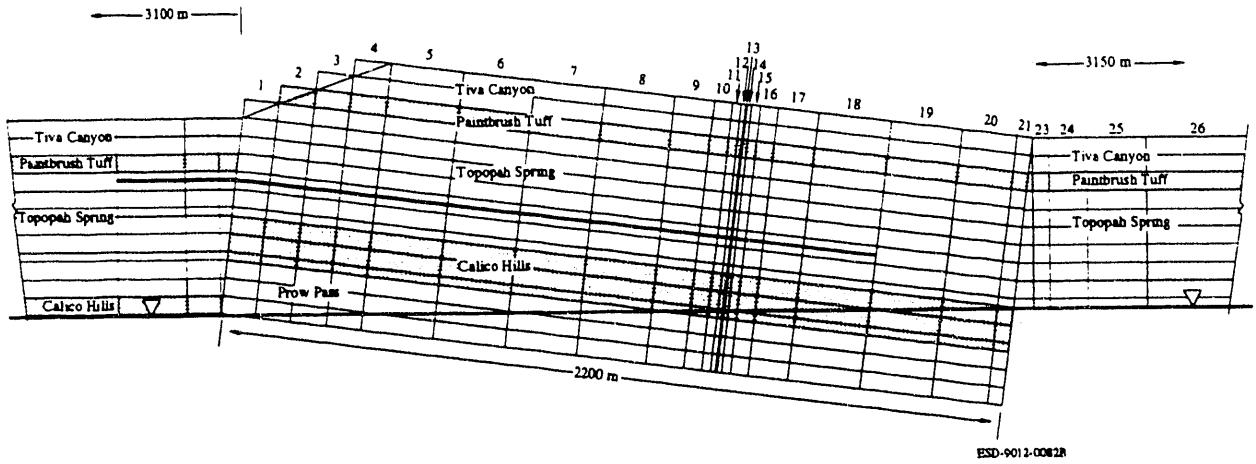

Figure 1 - Computational grid for two-dimensional east-west vertical section model of Yucca Mountain.

with the subscripts s and r denoting saturated and residual values, respectively. The parameter α may be considered as an empirical scaling parameter related to the capillary radius r_c by the capillary equation

$$r_c = \frac{(2\sigma\cos\theta)\alpha}{\rho g}, \qquad (3)$$

where σ is surface tension, θ is contact angle, ρ is water density, and g is the gravitational acceleration. In most applications, the number of empirical parameters is reduced by setting

$$m = 1 - \frac{1}{n} \qquad (4)$$

where the parameter (n−1) has the physical significance of a pore-size distribution index. Figure 2 shows a log-log plot of the saturated permeability k_s versus the capillary radius r_c for the three data sets of Yucca Mountain tuff, Apache Leap tuff, and Las Cruces soil. Note that the points for data sets span several orders of magnitude in both the saturated permeability and the capillary radius r_c (or capillary scaling factor α); yet among very different soil and rock media, there is a general trend that the mean value of saturated permeabilities is approximately proportional to the square of capillary radii. The straight line in Figure 2 is the classical Poiseuille equation for the permeability of a tube with radius r_c. Most of the data falls below the straight line, the vertical displacement of the data from the straight line may be interpreted as the effect of pore constrictivity and tortuosity relative to straight capillary tubes. A log-log plot[4] of the saturated permeability k_s versus the pore size distribution index (n−1) revealed no correlation between the mean values of these two parameters.

Based on the above observations of the correlation between the hydrological parameters of the soil and rock data, we construct the following conceptual model for the hydrological properties of the Ghost Dance Fault in this study. We hypothesize that the fault is a 'broken-up' version of the original formation, hence giving rise to saturated permeability which is considerably larger than that of the 'unbroken' formation. Two alternative conceptual representations of the faults are shown in Figure 3. Figure 3a shows the fault as composed of large pieces of original formation inter-

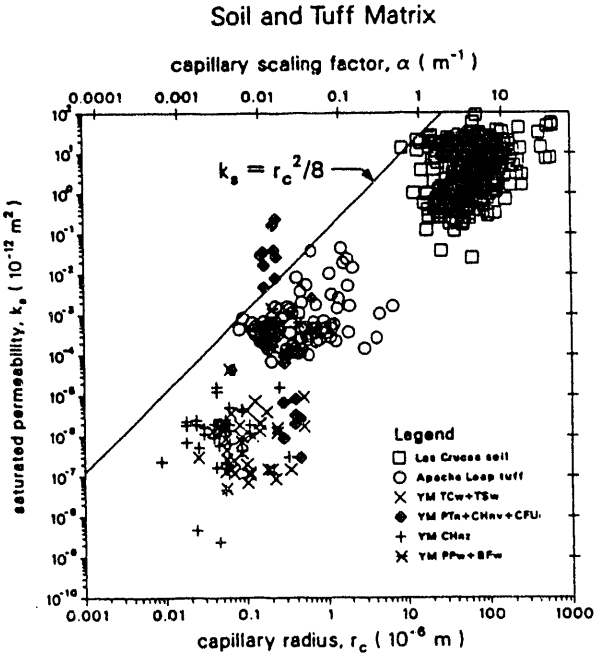

Figure 2 - Correlation between saturated permeability and capillary radius.

spersed among more finely broken-up material. Figure 3b shows the entire fault to consist of the finely broken-up material. Hence Figure 3a offers a double-porosity description of the fault while Figure 3b represents the fault as a single porous medium. We further assume that it is the finely broken-up material in Figure 3 which contribute to the enhanced saturated permeability in the faults. In the following, we shall label the large pieces of rubble in Figure 3a as 'unaltered', with reference to the hydrological properties of the original formation adjacent to the fault, and the finely broken-up part of the fault as 'altered'. If now a saturated permeability is assumed for the 'altered' medium in the fault, the correlations displayed in Figure 2 afford the rationale to derive the cap-

illary radius scaling parameter from the saturated permeability by $k_s=r_c^2/8$, neglecting the tortuosity correction, and in turn, the van Genuchten parameter α is obtained by means of Eq (3). Therefore the characteristic curves of the 'altered' medium in Ghost Dance Fault are assumed, except for the parameter α, to retain identical parameters (m, n, S_r, S_s) as those of the 'unaltered', which are those of the original formation adjacent to the fault. The parameter α will be scaled to the saturated permeability of the 'altered' medium, which is assumed to be 4.4×10^{-11} m^2. The choice of 4.4×10^{-11} m^2 is based on the information on fractures in the tuff units at Yucca Mountain. Klavetter and Peters[2] tabulate the fracture permeabilities of different units to range from 1.4×10^{-12} m^2 to 6.1×10^{-11} m^2. They also have a theoretical model for the fracture characteristics curve with an α value of 1.2851 m^{-1}, which convert to $k_s = 4.4 \times 10^{-11}$ m^2 by means of $k_s=r_c^2/8$. The saturated permeabilities for the nonwelded and welded matrix of the formation adjacent to the fault used in this study [5] are 1.9×10^{-18} m^2 for TSW and the TCW welded units, 1.8×10^{-14} m^2 for CHN and PTN nonwelded units, and 4.5×10^{-16} m^2 for PPW welded unit. The van Genuchten parameters used in this modeling study (samples TSW G4-6, PTN GU4-2, CHNV GU3-15) are derived from laboratory measurements[2,3] and have been applied to study the ambient gas movement and moisture migration,[5] as well as the performance assessment of a potential high-level nuclear waste repository at Yucca Mountain.[6] We assume that the welded units of Tiva Canyon and Prow Pass have the same van Genuchten parameters as the Topopah Spring unit. Figure 4 shows the measured capillary suction curves for the different layers, and the derived curves of their respective 'altered' fault material in these layers, based on scaling α according to the saturated permeability value of 4.4×10^{-11} m^2. Figure 5 shows the relative permeability k_{rl} characteristic curves for the different layers,

$$k_{rl} = \sqrt{S_e}\left[1-\left(1-S_e^{1/m}\right)^m\right]^2 \qquad (5)$$

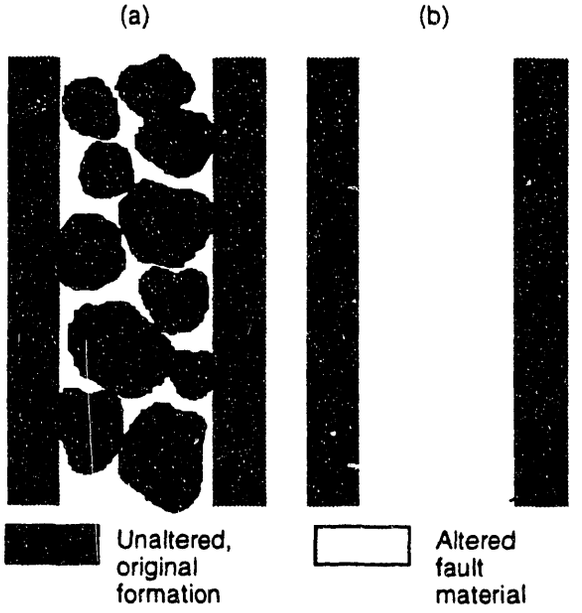

Figure 3 - Alternative conceptualization of the fault (a) double-porosity effective continuum, (b) single porosity medium.

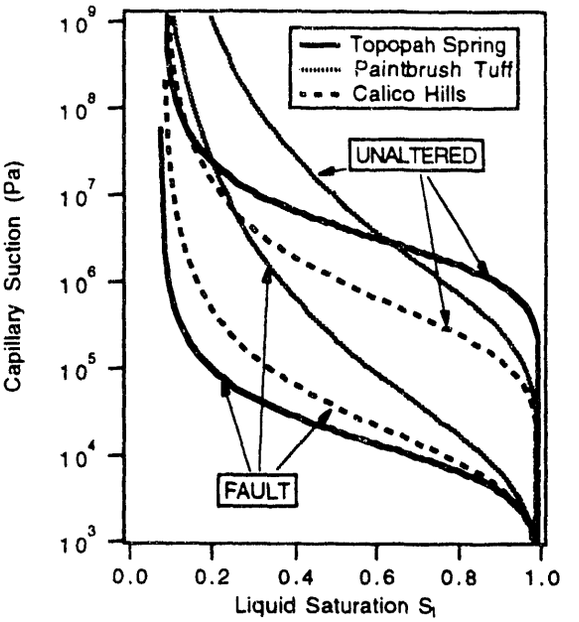

Figure 4 - The capillary suction characteristic curves for the stratigraphic units, including those of the 'altered' material in the fault zones.

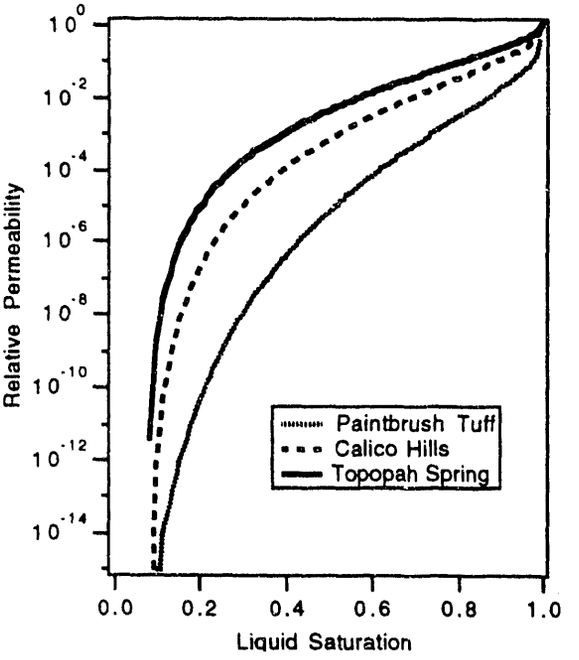

Figure 5 - The relative permeability characteristic curves for the stratigraphic units.

Since the relative permeability does not depend on α in the van Genuchten model, there is only one characteristic curve for each formation, irrespective of the 'altered' or the 'unaltered' material. For the double-porosity representation of the fault in Figure 3a, the characteristic curves of the fault are implemented in

the effective continuum approximation[5,7] where the 'altered' and 'unaltered' media are assumed to be in local capillary equilibrium, and the liquid saturation of the composite medium is expressed in terms of the fraction of void space (ϕ_u, ϕ_a) respectively of the 'unaltered' and 'altered' media, in terms of the total volume, and their respective liquid saturations (S_u, S_a).

$$S = \frac{S_u\phi_u + S_a\phi_a}{\phi_u + \phi_a} \qquad (6)$$

Weber and Bakker[8] have shown that typical values for fracture porosities in a large variety of rock types range from .001 to .02. We have chosen the upper limit .02 for the void fraction of the 'altered' material in the double porosity representation of the fault. The permeabilities of the composite medium at the effective continuum liquid saturation S are then

$$k_\beta(s) = \bar{k}_u k_{r\beta,u}(s_u) + \bar{k}_a k_{r\beta,a}(s_a)\,, \qquad (7)$$

where $\bar{k}_u$ and $\bar{k}_a$ stand for the saturated permeabilities, $k_{r\beta,u}$ and $k_{r\beta,a}$ the relative permeabilities, respectively of the 'unaltered' and 'altered' media; and β denotes either the gas or the liquid phase.

Simulations are performed for both the double-porosity (Figure 3a) and single porous medium (Figure 3b) representation of the fault. To study the effect of the Ghost Dance Fault on the fluid flow at Yucca Mountain, simulation is first performed for the reference case where columns 11 through 15 in Figure 1 (location of the Ghost Dance Fault if it were present) are given identical hydrological parameters ('unaltered' material) as their neighboring columns within each respective layer. For all simulations we apply at the land surface and the water table realistic boundary conditions of ambient pressures for both aqueous and gas phases, and natural geothermal gradients[5,6]. After the equilibrium natural state is obtained, we also simulate the system response to emplacement of high-level nuclear waste packages which are assumed to have the power decay output of a 10 year old waste, emplaced at an initial heat load of 57 kW per acre. Lawrence Berkeley Laboratory's general purpose multiphase fluid and heat flow simulator TOUGH2[9] was used in this work. TOUGH2 accounts for the multiphase fluid and heat flow processes including heat transfer by conduction and advection, phase change processes such as boiling and condensation, flow of liquid water and gas phase under gravity, capillary, and pressure forces, inter-diffusion of vapor and air, and vapor pressure lowering effects.

RESULTS

In the equilibrium natural state prior to waste emplacement, the gas flow field displays a subtle pattern of regional natural convection as a result of the geothermal gradient, the complex surface topography, and the tilting of the layers. The presence of the fault (with either representation in Figure 3) gives the result that an extra local convection cell appears within the fault zone. For the liquid flow field there is a general downward flow of water as a result of condensation of vapor counter to the upward flow of vapor driven by diffusion and buoyancy forces from the natural geothermal gradient. Figure 6 shows the profile with depth of the vertical (downward) component of liquid flow in the 80 m fault zone for the three cases: (1) the reference case where the fault is given identical properties as its adjacent formation, the 'unaltered' case, (2) the double-porosity representation of the fault zones as

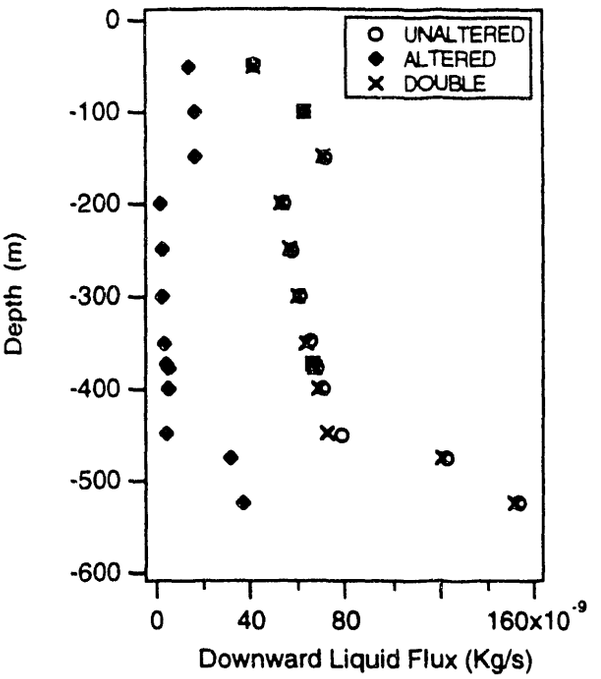

Figure 6 - The liquid flow profiles in the fault zone for fault properties (a) as unaltered from adjacent formation, (b) in the double-porosity representation and (c) single porosity 'altered' medium.

in Figure 3a, and (3) the single porosity representation of Figure 3b where the entire fault zone is given the 'altered' hydrological properties. We note that the results for the double-porosity representation of the fault are quite similar to that of the reference case where the fault is absent. These values of the vertical fluxes change at the interface between the different welded and non-welded layers: i.e., at 150 meter between the Paintbrush Canyon and the Topopah Spring, and at 475 meter between the Topopah Spring and the Calico Hills. The average value of the downward flux corresponds to about .04 mm/yr of water. For the single-porosity model of the fault, The values of the liquid flux is reduced by a factor of 50 in the Topopah Spring unit. This is understood as follows. The average ambient liquid saturation in the fault zone is on the order of 0.65 for the reference case. From Figure 4 it is seen that for the same capillary suction for which the liquid saturation S_u of the 'unaltered' formation is 0.65, the corresponding liquid saturation S_a for the 'altered' medium of the fault is much lower. And from Figure 5 we note the steep decrease of the liquid relative permeability values as the liquid saturation decreases. As a result, though the fault zone is assigned a saturated permeability many orders of magnitude larger than that of its adjacent formation, the opposing effect of the decreased relative permeability due to the lower liquid saturation S_a prevails and the actual liquid permeability in the fault turns out to be lower than that of the reference case. This gives rise to the smaller liquid flux in the fault when it is given the 'altered' hydrological properties, as shown in Figure 6. In addition to the equal or smaller magnitude of liquid flux down the fault as compared to the reference case, the simulated results of liquid flow vector field for both conceptual models of the fault zone are very similar to the reference case, and show no channeling of water into the fault. As for the

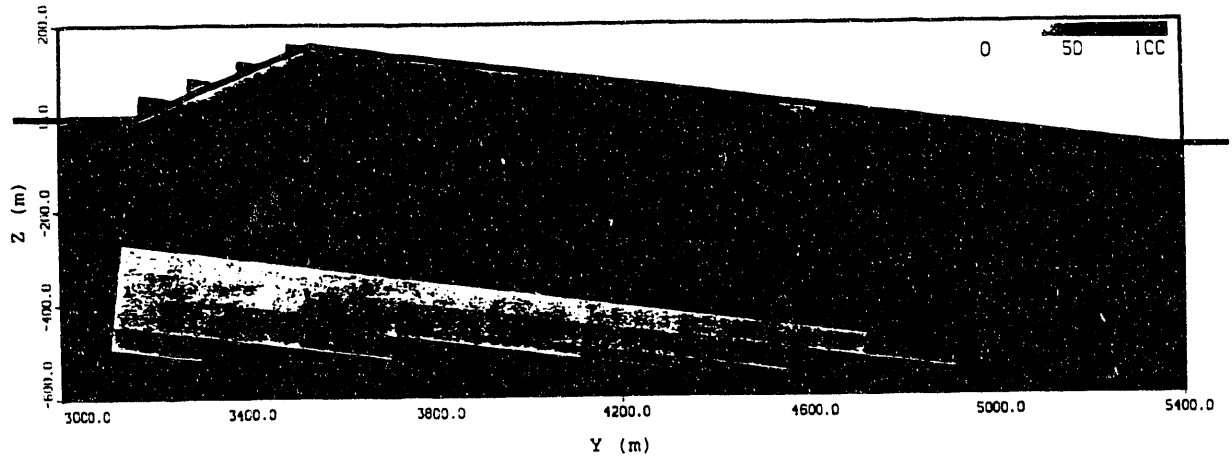

Figure 7 - Saturation distribution of the natural state for the double-porosity representation of the fault.

liquid saturation, the single-porosity model give rise to a much lower liquid saturation within the fault than its adjacent formation. In the double-porosity effective continuum conceptual representation of the fault, where the downward liquid flux is similar to the reference case, the fault is slightly drier than its adjacent formation, as shown in the liquid saturation distribution plot in Figure 7. The liquid saturation in the tuff formation apart from the fault are similar in both the reference case and the two simulations with fault properties.

Our simulated results therefore show that for both the single-porosity and double-porosity conceptualization of the fault zones, the fault plays little role in channeling water into itself, or in enhancing the flow of water down the fault, despite the very large saturated permeability assigned to it. On the other hand, by the very fact that the relative liquid permeability is low in the fault zones, it is to be expected that the gas phase permeability will be greatly enhanced by virtue of its saturated permeability being several orders larger than its adjacent formation. Indeed, since the fault provides the least resistive path for the gas phase flow, we note that the subtle gas flow pattern due to convection in the natural state is altered and a local convection cell forms in the fault zone. This is more clearly seen after the emplacement of waste when the flow becomes strongly heat-driven. In Figure 7 we show the gas phase flow field at 100 year after waste emplacement, for both the reference case (Figure 8a) where fault hydrological properties are absent, and the case where the fault is represented by the double-porosity effective continuum (Figure 8b). The location of the fault is defined by the most closely spaced vectors from the more refined gridding, and the repository extends slightly beyond the fault. Note the local convection cell of upward gas flow on the west and the downward flow in the east within the fault zone in case (b). Note also that the convection cell around right hand edge of the repository driven by the heat from the emplaced waste is more well formed in case (b) than in case (a), due to the larger gas permeability in the fault zone in case (b). It is clear from the figures that the gas flow field away from the fault are very similar in (a) and (b). The lengths of the vectors shown are proportional to the logarithm of the magnitude of the gas flux, and the largest vector in (b) is 5.26×10^{-7} kg/s-m^2, two orders of magnitude larger than the largest vector in (a). Simulation results for the single-porosity representation of the fault give very similar pattern as well as magnitude of the gas flow as in case (b).

CONCLUSIONS

Our study hypothesizes that the characteristic curves of the Ghost Dance Fault obey the same relationship between the saturated permeability and the capillary scaling parameter, as is observed for the data sets of Yucca Mountain tuffs, Apache Leap tuffs, and Las Cruces soil. Assuming the alternative models of single-porosity medium and a double-porosity medium where an effective continuum approximation is applicable, we find that a large saturated permeability assigned to the Ghost Dance Fault will play little role in channeling water into the fault, or in enhancing the flow of water down the fault. In fact, in the single-porosity representation of the fault the liquid flow in the fault zone is smaller than in the reference case where no fault hydrological properties are assumed. On the other hand, the large saturated permeability in the fault zone can greatly enhance gas flow after emplacement of waste. This may have implication on the transport of gaseous radio-nuclides such as C^{14}.

The simulation results show the behavior of fluid flow to be similar for the two alternative conceptual models (Figure 3) of the fault zone. How the fault affect the liquid and gas flow in the vicinity of the repository is critically controlled by the characteristic curves assumed for the fault zone. In our study we made an attempt to base our choice of the fault characteristic parameters on some scaling relationship between the saturated permeability and the capillary radius, as empirically observed for tuff. This kind of scaling produced a 'weaker' capillary suction for the material with the larger saturated permeability, as shown in Figure 4. And it is this kind of correlation between hydrological parameters which gives rise to our simulation results that the fault plays little role in affecting the liquid flow, but a more important role in enhancing the gas flow. However, if the hydrological parameters were such that a larger saturated permeability is coupled to a stronger capillary suction, contrary to the trend shown by the data in Figure 2, then one may expect the fault to play a more important role in providing a fast channel for the liquid flow. The magnitude of the

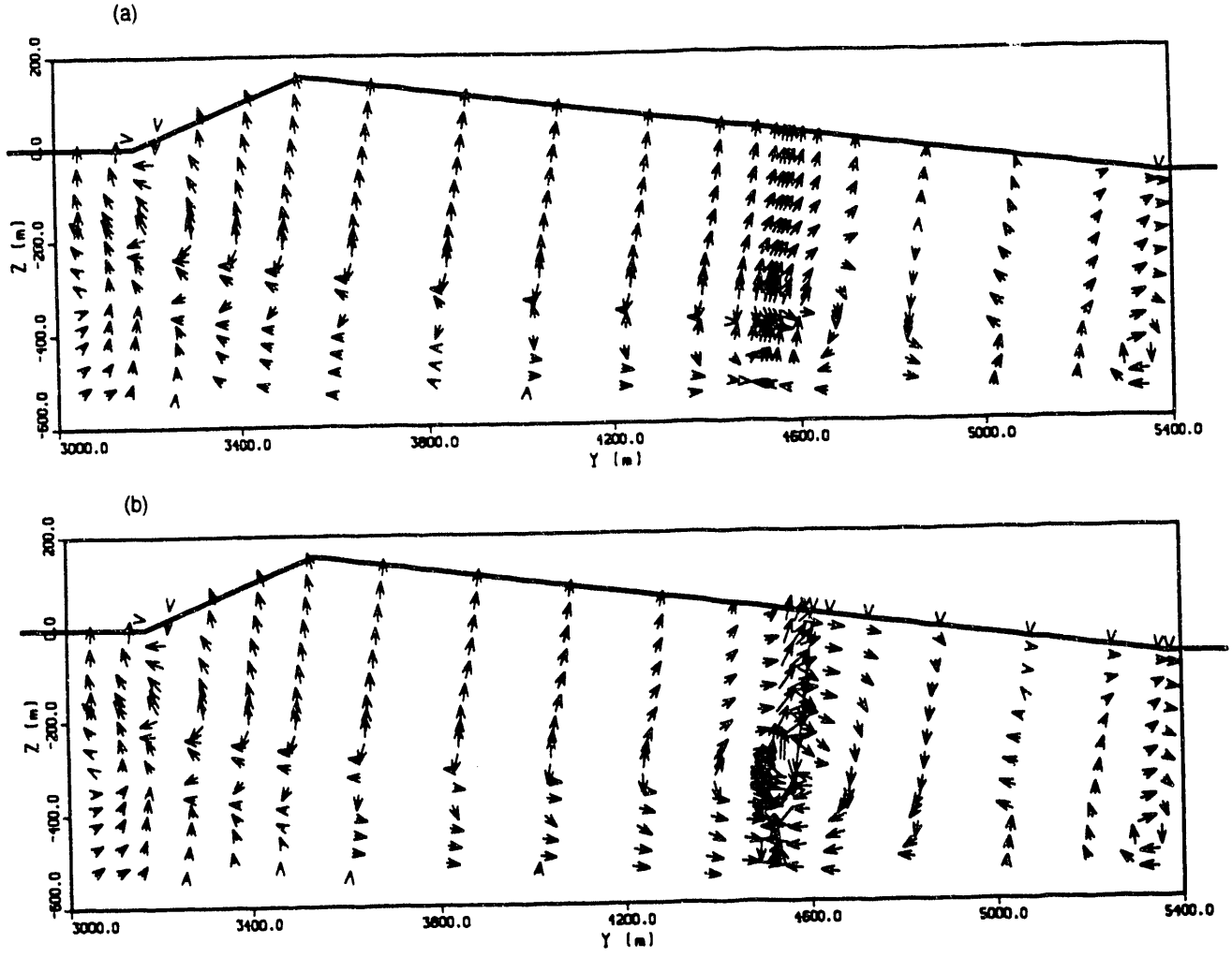

Figure 8 - The gas flow pattern at 100 year after waste emplacement for (a) reference case with no fault, (b) double-porosity representation of the fault.

liquid flow in the fault zone depends sensitively on the fault hydrological properties. The results of our study brings out the critical need for the experimental determination of the hydrological properties of the fault zone. Our study also focuses attention on the fact that hydrological parameters determined in the laboratory alone cannot definitively answer the question of the role of the fault in affecting fluid flow. We do need field measurements of gas flow and liquid saturation in the fault zone to determine the significance of the fault in controlling flow and transport at Yucca Mountain.

ACKNOWLEDGMENTS

The authors gratefully acknowledge support from the Director, Office of Civilian Radioactive Waste Management, the Yucca Mountain Site Characterization Project, U.S. Department of Energy, under contract NO. DE-AC03-76SF00098. Thanks are also due to C. F. Tsang and G. S. Bodvarsson for a review of the manuscript.

REFERENCES

1. R. W. SPENGLER, C. A. BRAUN, R. M. LINDEN, L. G. MARTIN, D. M. ROSS-BROWN, and R. L. BLACKBURN, "Structural Character of the Ghost Dance Fault, Yucca Mountain, Nevada," This issue.

2. E. A. KLAVETTER and R. R. PETERS, "Estimation of Hydrologic Properties of an Unsaturated Fractured Rock Mass," *Report SAND84-2642*, Sandia Nat. Lab. Albuquerque, NM (1986).

3. R. R. PETERS, E. A. KLAVETTER, I. J. HALL, S. C. BLAIR, P. R. HELLER and G. W. GEE, "Fracture and Matrix Hydrologic Characteristics of Tuffaceous Materials from Yucca Mountain, Nye County, Nevada," *Report SAND84-1471*, Sandia Nat. Lab. Albuquerque, NM, pp. 188 (1984).

4. J. S. Y. WANG. "Variations of Hydrological Parameters of Tuff and Soil," Proceedings of the Third International Conference HLRWM, Vol. 1, pp. 727-731 (1992).

5. Y. W. TSANG and K. PRUESS, "Further Modeling Studies of Gas Movement and Moisture Migration at Yucca Mountain, Nevada," *Report LBL-29127*, Lawrence Berkeley Laboratory, Berkeley, CA, May (1990).

6. K. PRUESS and Y. W. TSANG, "Modeling of Strongly Heat-driven Flow Processes at a Potential High-level Nuclear Waste Repository at Yucca Mountain, Nevada." This issue.

7. K. PRUESS, J. S. Y. WANG and Y. W. TSANG, "On Thermohydrologic Conditions Near High-level Nuclear Wastes Emplaced in Partially Saturated Fractured Tuff, Part 2., Effective Continuum Approximation," *Water Resour, Res., 26(6),* 1249-1261 (1990).

8. K. J. WEBER and M. BAKKER, "Fracture and Vuggy Porosity," paper presented at Proceedings 56th Annual Fall Technical Conference and Exhibition of the Soc. Pet. Eng., San Antonio, TX, October (1981).

9. K. PRUESS, "TOUGH2—A General-purpose Numerical Simulator for Multi-phase Fluid and Heat Flow," *Report LBL-29400*, Lawrence Berkeley Laboratory, Berkeley, CA, May (1991).

END

DATE
FILMED
7/8/93